

Journal of Biomedical Optics

BiomedicalOptics.SPIEDigitalLibrary.org

Photoacoustic lifetime imaging for direct *in vivo* tissue oxygen monitoring

Qi Shao
Shai Ashkenazi

Photoacoustic lifetime imaging for direct *in vivo* tissue oxygen monitoring

Qi Shao* and Shai Ashkenazi

University of Minnesota, Department of Biomedical Engineering, 312 Church Street SE, Minneapolis, Minnesota 55455, United States

Abstract. Measuring the partial pressure of oxygen (pO_2) in tissue may provide physicians with essential information about the physiological state of tissue. However, currently available methods for measuring or imaging tissue pO_2 have significant limitations, preventing them from being widely used in clinics. Recently, we have reported a direct and noninvasive *in vivo* imaging modality based on the photoacoustic lifetime which overcomes certain drawbacks of the existing methods. The technique maps the excited triplet state of oxygen-sensitive dye, thus reflecting the spatial and temporal distributions of tissue oxygen. Here, we present two studies which apply photoacoustic lifetime imaging (PALI) to monitor changes of tissue oxygen induced by external modulations. The first study modulates tissue oxygen by controlling the percentage of oxygen a normal mouse inhales. We demonstrate that PALI is able to reflect the change in oxygen level with respect to normal, oxygen-rich, and oxygen-poor breathing conditions. The second study involves an acute ischemia model using a thin thread tied around the hindlimb of a normal mouse to reduce the blood flow. PALI images were acquired before, during, and after the restriction. The drop of tissue pO_2 and recovery from hypoxia due to reperfusion were tracked and observed by PALI. © 2015 Society of Photo-Optical Instrumentation Engineers (SPIE) [DOI: 10.1117/1.JBO.20.3.036004]

Keywords: photoacoustic lifetime imaging; tissue oxygen; methylene blue; ischemia; reperfusion; hypoxia.

Paper 140713PRR received Oct. 30, 2014; accepted for publication Feb. 12, 2015; published online Mar. 6, 2015.

1 Introduction

In the human body, oxygen is transported from the lungs into the cells via the bloodstream. Oxygen plays a vital role in cellular metabolism. Oxygen partial pressure (pO_2), which results from the balance between oxygen delivery and its consumption, is a key component of the physiological state of tissue. Any imbalance in the oxygen levels, which may occur due to an altered supply or utilization of oxygen, will affect metabolic homeostasis and may lead to diseases.¹ Decrease in pO_2 , i.e., hypoxia, is strongly associated with diseases such as cancer,² peripheral artery disease,³ diabetes,⁴ and stroke.⁵ The interaction between the availability of oxygen and cellular function, including the signaling pathway of the hypoxia-inducible factor, has been studied intensively.⁶ In medicine, tissue oxygen is essential for diagnosis, therapy planning, and treatment monitoring for a range of diseases.⁷⁻⁹

The importance of tissue oxygen characterization raises the need for reliable measurement methods. Images of oxygen distribution may provide information about tissue hypoxia and evidence of oxygen availability in the circulatory system. Tissue oxygen can be assessed either indirectly or directly. Indirect methods include the measurement of oxygen saturation or parameters related to cell metabolism. Oxygen saturation can be obtained using techniques such as near-infrared spectroscopy¹⁰ and BOLD-MRI.¹¹ However, tissue oxygenation can be uncorrelated with blood oxygenation when there is insufficient blood perfusion such as in solid tumors¹² and implantations.¹³ Even though numerous hypoxia-related probes such as positron emission tomography¹⁴ and single-photon emission computed tomography¹⁵ have been developed, the interpretation of the images for identification of hypoxic regions remains

highly susceptible to the time delay between the injection of a contrast agent and image acquisition.¹⁶ The chemical and physical properties of oxygen enable a wide variety of direct methods for measuring pO_2 *in vivo*. Polarographic oxygen electrodes¹⁷ and fiber optic probes^{18,19} have been used in clinical practice. These probes are invasive and not capable of mapping (imaging) the oxygen content in tissue. Optical imaging methods including fluorescence quenching²⁰ and phosphorescence imaging²¹ suffer from low penetration depth due to the strong optical scattering in tissue. Magnetic-resonance-based methods (e.g., ¹⁹F MRI,²² electron paramagnetic resonance,²³ and proton-electron double resonance imaging²⁴) have long scanning times and, therefore, cannot generate real-time images. Moreover, other disadvantages including high costs and incompatibilities with implants and pacemakers make magnetic-resonance-based methods rarely implemented in clinical settings.

Evolved from phosphorescence lifetime imaging, photoacoustic lifetime imaging (PALI) is a novel method that directly reflects the spatial and temporal distributions of tissue oxygen.²⁵ PALI maintains the reliable sensing mechanism of oxygen-dependent decay after excitation. Instead of probing the transient optical emission, which is used in a range of commercially available medical and biological devices,²⁶⁻²⁹ PALI quantifies the same lifetime from excited state to ground state by probing the transient absorption.^{30,31} The sensing depth of lifetime imaging is thus largely increased by applying photoacoustic imaging. Photoacoustic imaging overcomes the diffusion limit of traditional optical methods by detecting ultrasound generated from light absorption.³² Penetration depth of photoacoustic imaging in tissue can reach up to a few centimeters.³³ By combining lifetime oxygen sensing and photoacoustic imaging, PALI is able to reveal the distribution of pO_2 with the resolution

*Address all correspondence to: Qi Shao, E-mail: shaox070@umn.edu

determined by an ultrasound transducer, typically less than 1 mm, and a penetration depth of about 15 mm.^{34–36} Even though lifetime-based photoacoustic methods enable direct measurement of pO_2 , they require perfusion of exogenous contrast agents into the region of interests, which may raise concerns such as biosafety and biocompatibility.³⁷ In comparison, spectroscopy-based photoacoustic imaging methods quantifying the oxygen saturation (SO_2) rely solely on hemoglobin as an endogenous contrast agent.^{38–40} These methods are easier to implement, however, they are insensitive to changes in oxygen transport and consumption in tissue. Poor correlations between oxygen saturation and tissue hypoxia have been observed in studies of prostate cancer,⁴¹ breast cancer,⁴² and rectal cancer.⁴³ These observations strongly suggest that there is a need for imaging methods that directly map tissue oxygen.

We have recently demonstrated the application of PALI to the imaging of tumor hypoxia in a small animal model.³⁴ The basic principles of PALI have been discussed in greater detail there. PALI consists of a series of excitation-probing pulse pairs. The pump pulse excites an oxygen-sensitive dye, and the probe pulse generates photoacoustic signals proportional to the transient absorption of the dye. These photoacoustic signals are recorded by an ultrasound array. The data acquired following each probing pulse are used to reconstruct a transient photoacoustic image corresponding to a specific pump-probe delay. The series of photoacoustic images is processed in a pixel-wise manner to extract the dynamics of transient absorption at each pixel location in the field of view. Pixel values at different time delays are fitted to an exponential decay function, and decay rates at each pixel are extracted and converted to pO_2 values using the Stern–Volmer equation.^{44,45} The pO_2 values of all pixels are then presented as a pO_2 distribution map. Data validation criteria have been defined to reject unreliable measurements. These include a threshold signal amplitude and a coefficient of determination of the exponential fit.

We use an oxygen-sensitive dye, methylene blue (MB), in our work. MB is a water-soluble dye that is widely used in clinical diagnostic and therapeutic applications^{46,47} primarily due to its low cytotoxicity and efficient clearance.^{48,49} MB has several advantages over other oxygen-sensitive dyes: (1) The safety and

toxicity of MB in humans have been widely studied and are well documented including an extensive formal toxicity study by the National Toxicology Program (NTP);⁵⁰ (2) MB can be efficiently (quantum yield for intersystem crossing $\eta_{ISC} = 0.52$) excited, and the excitation and probe wavelengths (650 and 810 nm) lie within the tissue optical windows; (3) the lifetime of MB is an intrinsic property and does not depend on its concentration (79.5 μs in oxygen-depleted solution⁵¹); (4) the lifetime is highly sensitive to pO_2 (the rate of collisions is higher than the relaxation rate of the excited state); and (5) it has been demonstrated that MB can be used as a photosensitizer in photodynamic therapy (PDT) to treat tumors, which would enable integration of PALI tissue oxygen monitoring with PDT.

2 Materials and Methods

2.1 Multimodal Imaging System

The imaging system allowed for three modes of operation: pulse-echo ultrasound imaging, photoacoustic imaging, and PALI. The main components of this system were two laser modules, an ultrasound system, and a computer, as shown in Fig. 1. The pump laser generated a wavelength of 650 nm to match the peak absorption of MB in its ground state to excited state transition. The pump laser system combined a pulsed Nd:YAG laser (Surelite I, Continuum), a third harmonics generation module, and an optical parametric oscillator (OPO; MagicPRISM, OPOTEK). The output wavelength of the second laser (probe laser) system was tuned to 810 nm to match the excited state triplet–triplet peak absorption of MB. The probe laser (Rainbow, OPOTEK) was a commercially integrated frequency-doubled Nd:YAG pulsed laser (Brilliant, Quantel) with an OPO unit. Both lasers operated at a 10-Hz repetition rate, with a pulse width of 5 ns and pulse energy of about 8 mJ. Light was combined and focused by a series of lenses and mirrors. Light intensities at the illumination spot were between 10 and 15 mJ/cm^2 (below the ANSI limit⁵²). Both lasers were externally triggered by a field-programmable gate array (FPGA) module (Saxo FPGA board, KNJN). The ultrasound system (OPEN system, Lecoer Electronique) was connected to a 64-element ultrasound

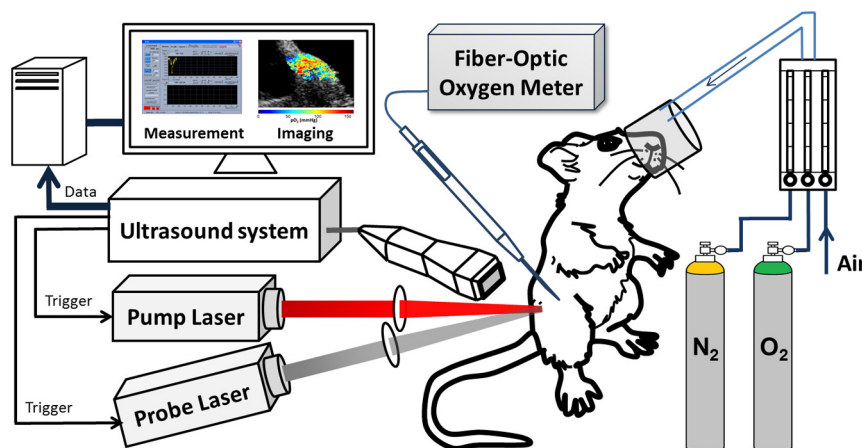


Fig. 1 Schematic of *in vivo* multimodal imaging system and breathing modulation model. The imaging system is capable of generating ultrasound, photoacoustic imaging, and PALI images using the same hardware. Two lasers illuminate the intended target region of the animal, and the generated ultrasound signals are acquired by a phased-array ultrasound transducer and then amplified, digitized, and processed in an ultrasound system. The percentage of oxygen the mouse inhales is controlled and the tissue oxygen near the imaging area is measured during the imaging process.

phased-array transducer (P7-4, ATL) as a transmitter–receiver in pulse–echo ultrasound imaging mode and as a receiver-only in photoacoustic and PALI modes. In all modes, signals from all channels were simultaneously digitized at a 12-bit resolution at a rate of 80 MHz.

Ultrasound images were obtained using the synthetic aperture imaging method^{53,54} described in Ref. 34. The total signal acquisition time for a complete scan was <1 s. Ultrasound images were generated to provide the anatomical structure of the hindlimb. The photoacoustic signal acquired by the ultrasound array was first averaged over 50 measurements to compensate for the fluctuations in the OPO output energy. A filtered backprojection algorithm was applied to reconstruct the photoacoustic images.^{55,56} A series of photoacoustic signals was obtained with pump-probe delays of 0.25 μ s, 0.5 μ s, 1 μ s, 2 μ s, 4 μ s, 8 μ s, and 100 ms. The triplet state lifetime was evaluated at each pixel by an exponential fit. The Stern–Volmer relationship⁴⁴ describing the lifetime as a function of pO_2 was used to convert lifetime to pO_2 . Data validation criteria have been defined to reject unreliable measurements. These include a threshold signal amplitude (< 10% of maximum) and a coefficient of determination ($R^2 > 0.4$) of the exponential fit. Only pixels that pass both criteria were shown in the final pO_2 map.

Normal mice (BALB/CJ, The Jackson Laboratory) were used for imaging. Before imaging, mice were anesthetized by ketamine (100 mg/kg) and xylazine (10 mg/kg). Hair on one side of the hindlimb was shaved and removed. MB (5 mM, about 5 spots, 50 μ L each spot) was injected subcutaneously at the hindlimb. The mouse was placed in an animal holder, with a labmade breathing apparatus mounted on the head to allow for free breathing. The breathing apparatus was connected to the flow-rate controller which mixes oxygen, nitrogen, and air. The concentration of oxygen inhaled by the animal was achieved by tuning the flow rate ratio of either oxygen or nitrogen with respect to the air. The total flow rate stayed at 120 ml/min for the entire experiment. Imaging experiments were conducted 15 min after the dye injection to allow for

sufficient dye distribution in the tissue by diffusion. The pO_2 of the hindlimb was also assessed by a commercial single-point oxygen probe. The device consisted of a retractable needle-type oxygen sensor (OXR50-OI, Pyroscience) and optical oxygen meter (Firesting O2, Pyroscience). The needle was placed close to the imaging area in order to obtain a simultaneous recording of the tissue, but also to avoid direct laser exposure and damage to the optical sensing tip, as shown in Figs. 1 and 2(d). All animal procedures and care were done using protocols approved by the University of Minnesota Institutional Animal Care and Use Committee (IACUC) in accordance with federally approved guidelines.

Three PALI images were taken under the condition of breathing in 21%, 80%, and then 10% of oxygen, with ultrasound images capturing the structure and without touching the mouse. For each condition, imaging started 1 min after switching conditions, so that the mouse was able to adjust to the new condition to ensure physiological stability during imaging. To avoid impairment of the animal's health, the total time of exposure to each gas mixture was limited to 4 min. After three imaging processes, the breathing tool was removed, and the mouse recovered from anesthesia in the open air and on a heat pad. The health status of the animal was monitored after the experiment, and no side effects were observed.

2.2 Ischemia Model

The same species of mice was used in this model. The animal was put on the same imaging platform and anesthetized as described in the breathing model. A PALI image was first taken under a normal condition. After the mouse under a normal physiological condition was imaged, acute ischemia of the hindlimb was induced by tightening a rubber band on the proximal side of the hindlimb, thus creating a localized ischemic condition on sites distal to the site of the occlusion. A second PALI image was taken under the ischemic condition. Immediately after the second image, the rubber band was removed, and a

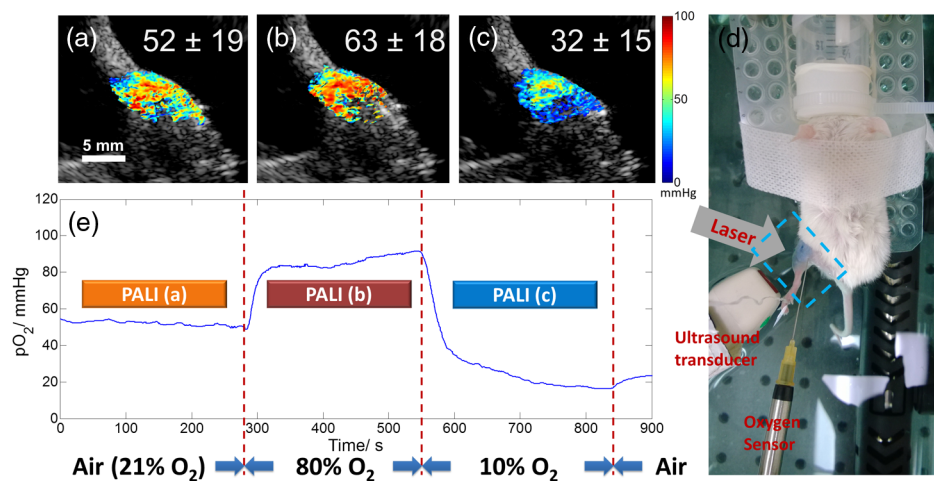


Fig. 2 PALI tracking of pO_2 during breathing modulation in the upper part of the hindlimb of a normal mouse. Combined US/PALI images are shown (pO_2 in mmHg color scale, ultrasound in 40-dB gray-scale): (a)–(c) tissue oxygen images reflecting tissue oxygen level under 21%, 80%, and 10% oxygen in mixture nitrogen, as their imaging periods indicated. (e) The values are given as the average \pm standard deviation for all valid pixel values displayed. (d) Photo of the mouse at imaging platform. The arrow indicates the direction of laser illumination and the blue dashed box shows the area of imaging shown in (a)–(c). (e) Simultaneous recording from the optical oxygen meter. Periods of gas mixture and PALI images are indicated.

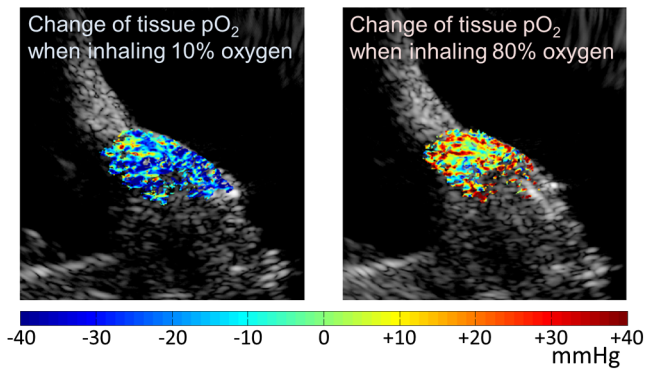


Fig. 3 Pixel-by-pixel-based relative changes in tissue pO_2 due to modulated inhalation of low oxygen (10%) and high oxygen (80%) contents, respectively. Changes are calculated with respect to image acquired with normal air breathing.

third PALI image was taken to capture the condition of reperfusion. The animal was under each condition (namely normal, ischemic, and postperfusion) for less than 20 min (including about 10 min of the imaging time).

3 Results

3.1 Breathing Modulation

PALI is able to reflect the change of oxygen level with respect to both oxygen-rich (80% O_2) and oxygen-poor (10% O_2) conditions to the normal oxygen level (21% O_2) in the air, as shown in Fig. 2. A high percentage (80%) of inhaled oxygen resulted in higher tissue oxygen levels. Furthermore, a low oxygen percentage (10%) resulted in hypoxic tissue. Both changes due to modulated inhalation are shown in Fig. 3. The PALI results were consistent with the oxygen probe single-point measurement.

3.2 Ischemia Model

The imaging results of the acute ischemia model are shown in Fig. 4. Even though the rubber band occlusion affected the

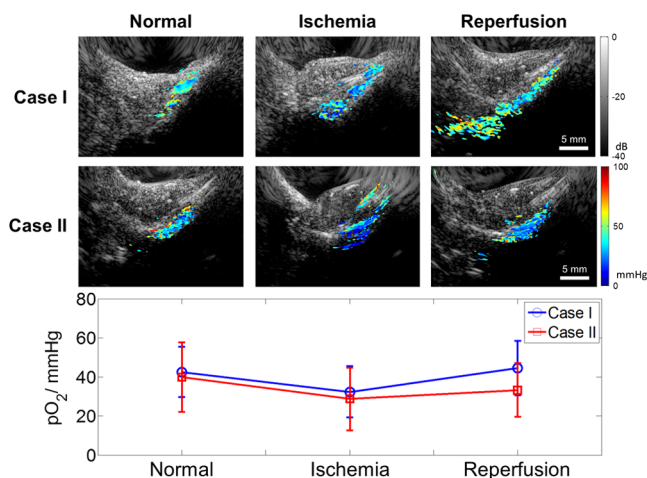


Fig. 4 PALI tracking of pO_2 during a blood-flow-restricting experiment in the upper part of hindlimb of normal mice. Combined US/PALI images are shown before (column under normal), during flow restriction (ischemia), and immediately after releasing the restriction (reperfusion). Cases I and II were experiments done on two mice. Statistics of the pixel values imaged are given by the average and error bars as standard deviation.

extent of tissue ischemic hypoxia of the two animals differently (mostly due to the differences in the tightness and location of the rubber band), the images clearly show the differences in tissue oxygen between normal, ischemic, and reperfused states in Fig. 4. From the color scale of PALI images, the decrease in the tissue oxygen level under ischemia was captured. When the rubber band was removed, the recovery of blood flow increased the tissue oxygen level compared with the ischemic status.

4 Conclusions and Discussions

We have demonstrated that PALI is able to reflect the change of oxygen levels in a direct and noninvasive manner. Tissue oxygen changes were induced by two methods and were both captured by our imaging modality. A single-point oxygen meter validated the imaging results. The changes of tissue oxygen obtained by PALI are highly correlated with the measurements obtained from the oxygen sensor. The increase of tissue oxygen due to high-inhaled oxygen (80%) was captured both in our PALI images (average pO_2 changed from 52 to 63 mmHg) and the oxygen sensor (from 52 ± 1 to 86 ± 3 mmHg). In addition, the drop of pO_2 values as a result of the low-oxygen (10%) breathing condition is observed from our PALI images (average of 32 mmHg) and confirmed by the direct measurement of oxygen sensor probe (drop to 24 ± 5 mmHg). The imaging system was able to visualize changes occurring within the time scale of a few minutes. This is valuable for rapidly identifying changes in pathophysiological conditions. The system was also able to capture the spatial distribution of pO_2 in a nondestructive manner compared with repeating single-point measurement. A multi-imaging modality (ultrasound, photoacoustic, and photoacoustic lifetime) was integrated due to the nature of their common ultrasound acquisition module. The multimodal capacity enables structural, functional, and molecular imaging with a single setup.

Restricted by the performance of our optical system, the current stage of our imaging modality has certain limitations. The laser system output (power at desired wavelength <100 mW) constrains the imaging area coverage, which has a surface area of about 2 cm^2 and a depth less than 1 cm. The variation of both laser intensity and low repetition rate (10 Hz) contributes to the relatively long-acquisition time necessary for PA signal averaging in order to get reliable readings. Specifically, the averaging of 50 measurements of acquired photoacoustic signal is used to improve the signal-to-noise ratio by 17 dB. This amounts to a total acquisition time of less than 3 min for a single PALI image. The resolution is determined by the ultrasound transducer, which is used for photoacoustic signal detection and, therefore, resembles that of a US imaging.^{57,58} In our system, the resolution is less than 0.5 mm by using a transducer with a bandwidth of 4 to 7 MHz. The pixel-to-pixel variations in pO_2 as depicted in PALI images are relatively high. In some cases, sharp changes of up to 100 mmHg are observed within a distance of less than 1 mm. It is difficult to ascertain which part of these variations reflects the true oxygen heterogeneity in tissue and which part should be attributed to measurement error. Previous phantom experiments have shown that the measurement error is well below 20%.³⁴ Differences in pO_2 values between the commercial oxygen probe and PALI images are likely attributed to the fact that the point of the probe measurement is not within the imaging area and to the heterogeneous nature of tissue oxygen. The tools and methods we presented

here could be applied to further explore the dynamics of tissue oxygen. It would allow detailed study of spatial and temporal changes in tissue oxygen in response to therapeutic treatments or other modulations. Further work is needed to better quantify the *in vivo* accuracy of the PALI oxygen imaging system.

PALI is very attractive for a wide range of clinical applications in which direct tissue oxygen assessment would improve therapy decision making and treatment planning. Examples include cancer treatments (radiotherapy and PDT) and treatments of diabetes-related ulcers. We anticipate that the ability to measure tissue oxygenation will enable physicians to better diagnose as well as to optimize treatment plans. A more comprehensive optimization of PALI is still required before its implementation into clinical applications could be developed. Substantial work is needed to further improve the imaging performance such as accuracy and speed. One of the methods to improve image acquisition speed is by adapting lasers with a higher repetition rate and lower energy fluctuation, thus largely reducing the time for averaging signals. Another possible way to reduce the time consumption of averaging is to have laser pulse energy monitored during the course of imaging, so that the intensity fluctuations of the lasers can be compensated. Other methods of light delivery, such as the use of minimally invasive, tissue-penetrating fiber diffusers, should be explored in order to extend the applicability of PALI into an even broader range of clinical applications.

Acknowledgments

The authors thank Ekaterina Morgounova for constructive discussions. The authors appreciate Kelsey Pfllepsen's close reading of the manuscript and support from the Center of Writing, University of Minnesota. This work was sponsored by NIH R21 EB016763, R21 CA135027, NIH R01 CA183749, and IME Cancer Animal Core Lab, University of Minnesota. Qi Shao was supported by Doctoral Dissertation Fellowship, University of Minnesota.

References

1. D. Abele, "The radical life-giver," *Nature* **420**(6911), 27 (2002).
2. M. Hockel and P. Vaupel, "Tumor hypoxia: definitions and current clinical, biologic, and molecular aspects," *J. Natl. Cancer Inst.* **93**(4), 266–276 (2001).
3. U. K. Franzcek et al., "Transcutaneous pO₂ measurements in health and peripheral arterial occlusive disease," *Surgery* **91**(2), 156–163 (1982).
4. J. Ditzel, "Oxygen-transport impairment in diabetes," *Diabetes* **25**(Suppl 2), 832–838 (1976).
5. D. Laurent et al., "Effects of heart rate on coronary flow and cardiac oxygen consumption," *Am. J. Physiol.* **185**(2), 355–364 (1956).
6. C. J. Schofield and P. J. Ratcliffe, "Oxygen sensing by HIF hydroxylases," *Nat. Rev. Mol. Cell Biol.* **5**(5), 343–354 (2004).
7. D. S. Vikram, J. L. Zweier, and P. Kuppusamy, "Methods for noninvasive imaging of tissue hypoxia," *Antioxid. Redox Signaling* **9**(10), 1745–1756 (2007).
8. H. W. Hopf et al., "Wound tissue oxygen tension predicts the risk of wound infection in surgical patients," *Arch. Surg.* **132**(9), 997–1004 (1997).
9. N. Chang et al., "Direct measurement of wound and tissue oxygen-tension in postoperative-patients," *Ann. Surg.* **197**(4), 470–478 (1983).
10. A. Villringer et al., "Near-infrared spectroscopy (NIRS)—a new tool to study hemodynamic-changes during activation of brain-function in human adults," *Neurosci. Lett.* **154**(1–2), 101–104 (1993).
11. P. V. Prasad, R. R. Edelman, and F. H. Epstein, "Noninvasive evaluation of intrarenal oxygenation with BOLD MRI," *Circulation* **94**(12), 3271–3275 (1996).
12. J. G. Rajendran and K. A. Krohn, "Imaging hypoxia and angiogenesis in tumors," *Radiol. Clin. North Am.* **43**(1), 169 (2005).
13. T. M. Suszynski et al., "Assessment of tissue-engineered islet graft viability by fluorine magnetic resonance spectroscopy," *Transplant. Proc.* **43**(9), 3221–3225 (2011).
14. B. J. Krause et al., "PET and PET/CT studies of tumor tissue oxygenation," *Q. J. Nucl. Med. Mol. Imaging* **50**(1), 28–43 (2006).
15. R. C. Urtasun et al., "Measurement of hypoxia in human tumours by non-invasive SPECT imaging of iodoazomycin-araboside," *Br. J. Cancer Suppl.* **27**, S209–S212 (1996).
16. J. L. Tatum et al., "Hypoxia: importance in tumor biology, noninvasive measurement by imaging, and value of its measurement in the management of cancer therapy," *Int. J. Radiat. Biol.* **82**(10), 699–757 (2006).
17. P. L. Olive, J. P. Banath, and C. Aquino-Parsons, "Measuring hypoxia in solid tumours—is there a gold standard?," *Acta Oncologica* **40**(8), 917–923 (2001).
18. J. R. Griffiths and S. P. Robinson, "The OxyLite: a fibre-optic oxygen sensor," *Br. J. Radiol.* **72**(859), 627–630 (1999).
19. I. A. Barbazetto et al., "Oxygen tension in the rabbit lens and vitreous before and after vitrectomy," *Exp. Eye Res.* **78**(5), 917–924 (2004).
20. W. Zhong, P. Urayama, and M. A. Mycek, "Imaging fluorescence lifetime modulation of a ruthenium-based dye in living cells: the potential for oxygen sensing," *J. Phys. D: Appl. Phys.* **36**(14), 1689–1695 (2003).
21. R. D. Shonat et al., "Oxygen distribution in the retinal and choroidal vessels of the cat as measured by a new phosphorescence imaging method," *Appl. Opt.* **31**(19), 3711–3718 (1992).
22. U. Noeth et al., "19F-MRI *in vivo* determination of the partial oxygen pressure in perfluorocarbon-loaded alginate capsules implanted into the peritoneal cavity and different tissues," *Magn. Reson. Med.* **42**(6), 1039–1047 (1999).
23. M. Elas et al., "Quantitative tumor oxymetric images from 4D electron paramagnetic resonance imaging (EPRI): methodology and comparison with blood oxygen level-dependent (BOLD) MRI," *Magn. Reson. Med.* **49**(4), 682–691 (2003).
24. T. Liebgott et al., "Proton electron double resonance imaging (PEDRI) of the isolated beating rat heart," *Magn. Reson. Med.* **50**(2), 391–399 (2003).
25. S. Ashkenazi et al., "Photoacoustic probing of fluorophore excited state lifetime with application to oxygen sensing," *J. Biomed. Opt.* **13**(3), 034023 (2008).
26. Ocean Optics, "Oxygen Probes and Fibers," 2015, <http://oceanoptics.com/product-category/oxygen-probes-and-fibers/> (27 February 2015).
27. Oxford Optronix, "OxyLite Dissolved Oxygen Monitors," 2015, <http://www.oxford-optronix.com/product20/page501/Tissue-Vitality-Monitoring/Oxygen-Monitors/OxyLite-.html> (27 February 2015).
28. PreSens Precision Sensing GmbH, "Sensor Probes," 2015, <http://www.presens.de/products/category/category/sensor-probes.html> (27 February 2015).
29. Pyro Science, "Overview Optical Oxygen Probes," 2015, <http://www.pyro-science.com/overview-fiber-optic-oxygen-sensors.html>.
30. S. Ashkenazi, "Photoacoustic lifetime imaging of dissolved oxygen using methylene blue," *J. Biomed. Opt.* **15**(4), 040501 (2010).
31. A. Ray et al., "Lifetime-based photoacoustic oxygen sensing *in vivo*," *J. Biomed. Opt.* **17**(5), 057004 (2012).
32. M. H. Xu and L. H. V. Wang, "Photoacoustic imaging in biomedicine," *Rev. Sci. Instrum.* **77**(4), 041101 (2006).
33. G. Ku and L. V. Wang, "Deeply penetrating photoacoustic tomography in biological tissues enhanced with an optical contrast agent," *Opt. Lett.* **30**(5), 507–509 (2005).
34. Q. Shao et al., "In vivo photoacoustic lifetime imaging of tumor hypoxia in small animals," *J. Biomed. Opt.* **18**(7), 076019 (2013).
35. Q. Shao et al., "Mapping tissue oxygen *in vivo* by photoacoustic lifetime imaging," *Proc. SPIE* **8581**, 85811S (2013).
36. Q. Shao et al., "Noninvasive tumor oxygen imaging by photoacoustic lifetime imaging integrated with photodynamic therapy," *Proc. SPIE* **8931**, 89310H (2014).
37. D. Wu et al., "Contrast agents for photoacoustic and thermoacoustic imaging: a review," *Int. J. Mol. Sci.* **15**(12), 23616–23639 (2014).
38. J. Laufer et al., "In vitro measurements of absolute blood oxygen saturation using pulsed near-infrared photoacoustic spectroscopy: accuracy and resolution," *Phys. Med. Biol.* **50**(18), 4409–4428 (2005).

39. J. Yao et al., "Label-free oxygen-metabolic photoacoustic microscopy *in vivo*," *J. Biomed. Opt.* **16**(7), 076003 (2011).
40. H. F. Zhang et al., "Imaging of hemoglobin oxygen saturation variations in single vessels *in vivo* using photoacoustic microscopy," *Appl. Phys. Lett.* **90**(5), 053901 (2007).
41. D. Carnell et al., "Evaluation of prostate gland hypoxia with quantified BOLD MRI: updated results from a correlated histological study," in *Proc. Int. Society of Magnetic Resonance in Medicine*, Vol. 13, p. 270 (2005).
42. A. Padhani et al., "An investigation of histological and DC-MRI correlates of intrinsic susceptibility contrast relaxivity (R_2^*) in human breast cancer," in *Proc. Int. Society of Magnetic Resonance in Medicine*, Vol. 13, p. 1845 (2005).
43. G. Atkin et al., "Dynamic contrast-enhanced magnetic resonance imaging is a poor measure of rectal cancer angiogenesis," *Br. J. Surg.* **93**(8), 992–1000 (2006).
44. J. M. Vanderkooi and D. F. Wilson, "A new method for measuring oxygen concentration in biological systems," in *Oxygen Transport to Tissue VIII*, pp. 189–193, Springer (1986).
45. D. A. Dunn, V. H. Lin, and I. E. Kochevar, "The role of ground-state complexation in the electron-transfer quenching of methylene-blue fluorescence by purine nucleotides," *Photochem. Photobiol.* **53**(1), 47–56 (1991).
46. R. Kiesslich et al., "Methylene blue-aided chromoendoscopy for the detection of intraepithelial neoplasia and colon cancer in ulcerative colitis," *Gastroenterology* **124**(4), 880–888 (2003).
47. J. P. Tardivo et al., "Methylene blue in photodynamic therapy: from basic mechanisms to clinical applications," *Photodiagn. Photodyn. Ther.* **2**(3), 175–191 (2005).
48. J. Clifton, II and J. B. Leikin, "Methylene blue," *Am. J. Ther.* **10**(4), 289–291 (2003).
49. G. C. Buehring and H. M. Jensen, "Lack of toxicity of methylene blue chloride to supravivally stained human mammary tissues," *Cancer Res.* **43**(12 Pt 1), 6039–6044 (1983).
50. P. National Toxicology, "Toxicology and carcinogenesis studies of methylene blue trihydrate (Cas No. 7220-79-3) in F344/N rats and B6C3F1 mice (gavage studies)," *Natl. Toxicol. Program Tech. Rep. Ser.* **540**, 1–224 (2008).
51. M. Gonzalez-Bejar et al., "Methylene blue encapsulation in cucurbit 7 uril: laser flash photolysis and near-IR luminescence studies of the interaction with oxygen," *Langmuir* **25**(18), 10490–10494 (2009).
52. ANSI Laser Institute of America, *American National Standard for Safe Use of Lasers: ANSI Z136.1-2000*, American National Standards Institute, New York (2000).
53. I. Trots, A. Nowicki, and M. Lewandowski, "Synthetic transmit aperture in ultrasound imaging," *Arch. Acoust.* **34**(4), 685–695 (2009).
54. J. A. Jensen et al., "Synthetic aperture ultrasound imaging," *Ultrasonics* **44**, E5–E15 (2006).
55. Y. Xu et al., "Reconstructions in limited-view thermoacoustic tomography," *Med. Phys.* **31**(4), 724–733 (2004).
56. P. Burgholzer et al., "Exact and approximative imaging methods for photoacoustic tomography using an arbitrary detection surface," *Phys Rev E Stat Nonlin Soft Matter Phys* **75**(4 Pt 2), 046706 (2007).
57. A. Buehler et al., "Three-dimensional optoacoustic tomography at video rate," *Opt. Express* **20**(20), 22712–22719 (2012).
58. S. A. Ermilov et al., "Laser optoacoustic imaging system for detection of breast cancer," *J. Biomed. Opt.* **14**(2), 024007 (2009).

Qi Shao received his BS degree in biomedical engineering from Zhejiang University, Hangzhou, China. He is currently a PhD candidate in the Department of Biomedical Engineering, University of Minnesota, Minneapolis, Minnesota, USA. He is involved in developing techniques for optical functional and molecular imaging. He is also serving the IEM Animal Cancer Core Lab. His current research interests include biomedical imaging, instrumentation, cancer therapy, immunomodulation, and magnetic nanoparticle.

Shai Ashkenazi received his BSc in physics from the Technion Israel Institute of Technology, Haifa, Israel, in 1988, and his PhD degree in physics from the Weizmann Institute of Science, Rehovot, Israel, in 1997. In 2003, he moved to the University of Michigan as a research scientist. In 2008, he joined the Biomedical Engineering Department at the University of Minnesota, where he is currently an associate professor. His research interests include biomedical photonics, photoacoustics, and ultrasound imaging.